JOURNAL OF GEOPHYSICAL RESEARCH, VOL. 114, C06022, doi:10.1029/2008JC005081, 2009

A numerical study of circulation in a coastal reef-lagoon system

Ryan J. Lowe,[1] James L. Falter,[2] Stephen G. Monismith,[3] and Marlin J. Atkinson[2]

Received 13 August 2008; revised 19 December 2008; accepted 18 March 2009; published 24 June 2009.

[1] A coupled wave-circulation numerical model was used to simulate the distribution of wave energy, as well as the circulation induced by wave breaking, wind, and tidal forcing, within a coral reef system in Kaneohe Bay, Oahu, Hawaii. Modeled wave, current, and wave setup fields were compared with field measurements collected on the forereef, reef flat, and reef channels and in the lagoon over a 4-week period. The predicted wave height transformation across the reef-lagoon system was in good agreement with field observations, using single-parameter (spatially uniform) values to describe both wave-breaking and frictional dissipation. The spatial distribution of the resulting wave setup field drove a persistent wave-driven flow across the reef flat that returned to the ocean through two deeper channels in the reef. Both the magnitude and direction of these currents were well described using a spatially uniform hydraulic roughness length scale. Notably, the model lends support to field observations that setup within the coastally bounded lagoon was a substantial fraction of the maximum setup on the reef ($\sim$60–80%), which generated relatively weak cross-reef wave-driven flows ($\sim$10–20 cm s^{-1}) compared with reefs having mostly unbounded lagoons (e.g., many atolls and barrier reefs). Numerical experiments conducted using Lagrangian particle tracking revealed that residence times within Kaneohe Bay are extremely heterogeneous, typically ranging from <1 day on the reef to >1 month within its sheltered southern lagoon.

Citation: Lowe, R. J., J. L. Falter, S. G. Monismith, and M. J. Atkinson (2009), A numerical study of circulation in a coastal reef-lagoon system, *J. Geophys. Res.*, *114*, C06022, doi:10.1029/2008JC005081.

1. Introduction

[2] Circulation controls a variety of key processes in coral reef systems, including the transport and dispersal of larval fish and corals [e.g., *Kraines et al.*, 2001; *Lugo-Fernandez et al.*, 2001], nutrient delivery to reef organisms [e.g., *Atkinson and Bilger*, 1992; *Yahel et al.*, 1998] and sediment transport [e.g., *Kench and Brander*, 2006; *Storlazzi et al.*, 2004]. However, compared to similar nearshore flows on beaches (e.g., see the review by *MacMahan et al.* [2006]), comparatively little work has focused on predicting circulation on reefs, whose broader morphological category could include not just living coral reefs, but also relict limestone platforms and other submerged rock formations. While reefs have some similarities to beaches (e.g., their flows are ultimately driven by the same physical mechanisms), they do have at least two fundamental differences: (1) the bottom of reefs is often much rougher than sandy beds and (2) the reef bathymetry itself is often considerably more complex than sloping beaches. As a result, we do not yet know the extent to which existing theories and numerical modeling techniques developed and tested on beaches can be successfully extended to studies of reef circulation.

[3] Circulation on reefs can be driven by a number of mechanisms, including waves, tides, wind, and buoyancy effects [*Andrews and Pickard*, 1990]. The relative importance of each mechanism varies between reefs and is a function of both a reef's morphology and the meteorological and oceanic forcing conditions at the site. For a coral reef system, the morphology is often defined as having the following distinctive features (e.g., Figure 1b): a sloping forereef, a shallow reef flat, and a relatively deep lagoon. Although winds [*Pinazo et al.*, 2004; *Yamano et al.*, 1998], tides [*Douillet et al.*, 2001; *Kitheka*, 1997] and buoyancy effects [*Monismith et al.*, 2006] can play a dominant role in the circulation of some reefs, wave breaking has long been recognized as the dominate forcing mechanism within many wave-exposed reef systems [e.g., *Angwenyi and Rydberg*, 2005; *Hench et al.*, 2008; *Kraines et al.*, 1998; *Lugo-Fernandez et al.*, 2004; *Symonds et al.*, 1995]. This forcing is provided by wave breaking on the forereef which causes a local increase in the mean sea level ("wave setup") on the reef, establishing a pressure gradient that drives cross-reef mean flows.

[4] To predict wave-driven flows on reefs, a number of simplified one-dimensional (1D) analytical models have been proposed. All assume an idealized reef depth profile and then utilize a simple 1D wave transformation model to estimate maximum wave setup due to radiation stress gradients in the surf zone [e.g., *Gourlay and Colleter*,

[1]School of Earth and Environment, University of Western Australia, Crawley, Western Australia, Australia.
[2]Hawai'i Institute of Marine Biology, University of Hawai'i, Kaneohe, Hawaii, USA.
[3]Environmental Fluid Mechanics Laboratory, Stanford University, Stanford, California, USA.

0148-0227/09/2008JC005081$09.00

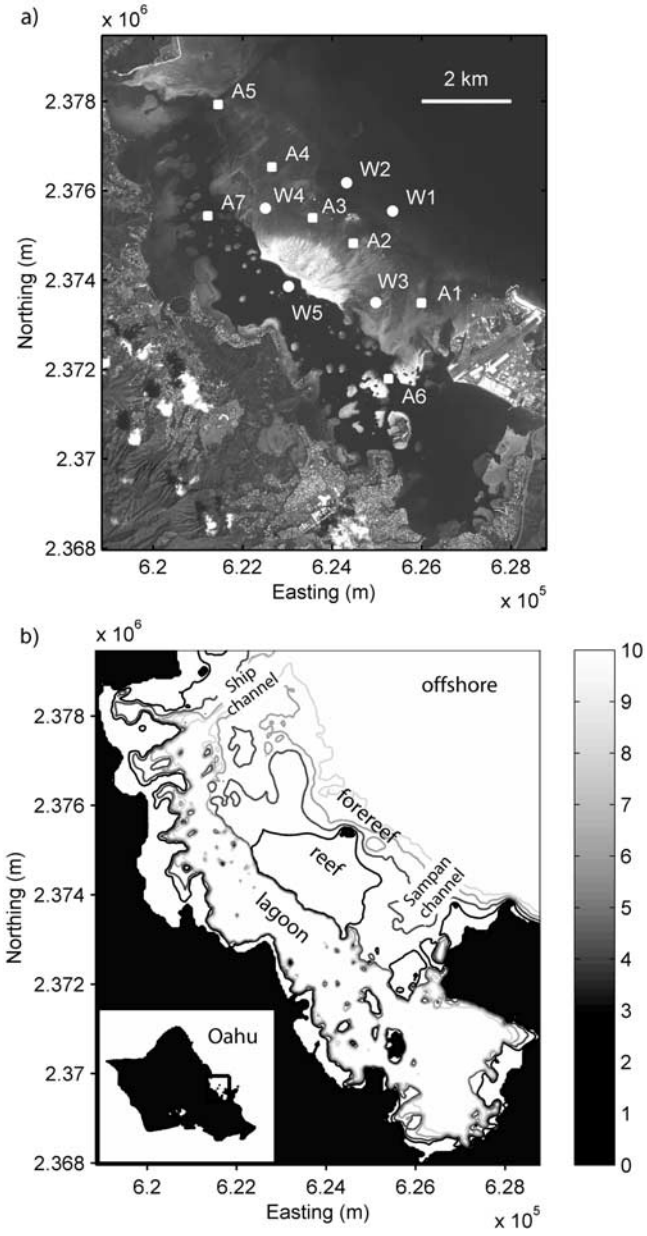

Figure 1. Kaneohe Bay, Oahu, Hawaii. (a) Aerial photograph with the instrument sites used to validate the model superimposed (Quickbird image courtesy of DigitalGlobe©) and (b) bathymetry contours (only depths up to 10 m shown) highlighting the dominant morphological features.

2005; *Hearn*, 1999; *Symonds et al.*, 1995]. The magnitude of the wave-driven flow is thus controlled by the water level difference between the surf zone and the lagoon. To achieve an analytical solution, existing 1D reef models have assumed that wave setup in the lagoon is negligible, making these models particularly appropriate for atolls and barrier reefs having lagoons that connect freely to the open ocean. However, many reefs (e.g., fringing reefs) have enclosed lagoons in which exchange with the surrounding ocean is often restricted by friction through relatively narrow gaps (channels) in the reef (Figure 1b). Lagoon setup in these systems may not be negligible, since water level differences between the lagoon and ocean must be present to return water entering the lagoon back to the ocean through channels formed in the reef [*Lowe et al.*, 2009]. As a result, these coastal reef wave-driven flows are inherently two dimensional, as their overall dynamics may also be strongly influenced by the momentum balances associated with these lagoon-channel return flows.

[5] Some two-dimensional (2D) and three-dimensional (3D) numerical models have been applied to reef systems. A clear advantage of these approaches is that there is no need to simplify the reef morphology into a single representative 1D profile. Furthermore, the circulation of most reef systems is driven by a combination of forcing mechanisms (e.g., not merely wave breaking), and the relative importance of these mechanisms may vary spatially and temporally throughout a system. The complex interactions between these different forcing mechanisms can only be fully explored through the use of these 2D and 3D numerical models. Although several reef modeling studies have focused on wind-driven and tidally driven flows [e.g., *Douillet et al.*, 2001; *Luick et al.*, 2007; *Tartinville et al.*, 1997], a few have also considered the effects of breaking waves [*Hearn*, 1996; *Kraines et al.*, 1998, 1999; *Prager*, 1991]. However, to generate wave-driven currents, these numerical models have typically prescribed the setup generated along the reef crest using predictions from simple analytical wave transformation models, i.e., similar to those used in the 1D analytical reef models discussed above. Over the past decade, a number of fully coupled wave-circulation numerical models have also been developed to predict wave-driven flows in nearshore environments; while these models have been widely validated using field data collected on sandy beaches, these coupled numerical models have yet to be extensively tested on reefs.

[6] In this study we apply a 3D coupled wave-circulation model to the morphologically complex coral reef system in Kaneohe Bay, Hawaii (Figure 1), in order to test the skill of the model to replicate wave heights, setup and currents, as observed during an extensive field study reported by *Lowe et al.* [2009], over a one month period. Although buoyancy effects may sometimes influence lagoon circulation, for example, because of extreme freshwater discharge into the lagoon during storms, such forcing is not considered here. For the present study, we use a version of Delft3D which iteratively couples currents with wave transformations simulated by the numerical wave model SWAN [*Booij et al.*, 1999]. This approach is very similar to recent adaptations of SWAN to other ocean circulation models such as POM [*Newberger and Allen*, 2007] and ROMS [*Warner et al.*, 2008]. This paper is organized as follows. In section 2, a description of the study site, field observations and model configuration is presented. In section 3, hindcast model predictions are quantitatively compared with field observations. In section 4, the relative importance of the various forcing mechanisms to residence times in Kaneohe Bay is evaluated by conducting a series of numerical experiments using Lagrangian particle tracking, with the range of forcing chosen on the basis of historical conditions measured at this

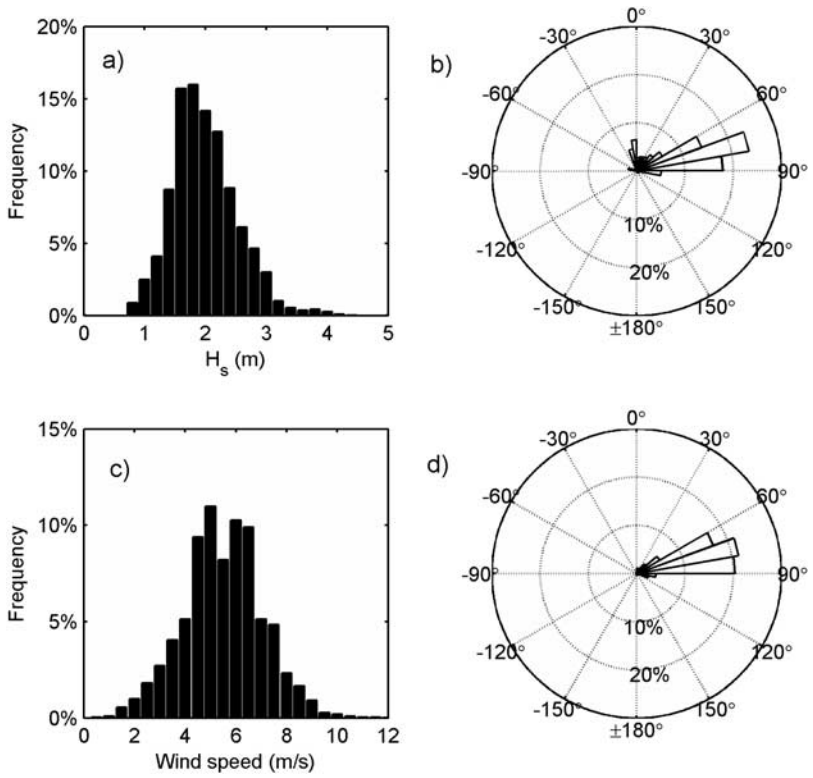

Figure 2. Historical wave and wind conditions at Kaneohe Bay, recorded during 2005–2006. Histogram of (a) significant wave height and (b) peak wave direction measured by the offshore wave buoy off Mokapu Point. Histogram of (c) wind speed and (d) wind direction recorded on Mokapu peninsula.

site. Finally, the discussion of the model results and a summary of conclusions are presented in sections 5 and 6.

2. Methods

2.1. Site Description and Climatology

[7] Kaneohe Bay (Figure 1), located on the northeast coast of Oahu, Hawaii (21°29′ N, 157°48′ W), is the largest sheltered body of water in the Hawaiian Islands (along shore length ~13 km; cross shore width ~4 km). A ~6 km long by ~2 km wide, shallow (<3 m) reef platform extends over much of the area, and is covered by various reef organisms (primarily macroalgae but some coral), coral rubble, and sand. A ~1–2 km wide lagoon (10–15 m depth) separates the reef from shore, with a bottom composed mostly of sands and muds. Distributed throughout the interior of the lagoon are a large number of coral patch reefs that rise to within 1 m of the surface (see Figure 1). Water inside the lagoon exchanges with the ocean through two main channels: the partially dredged Ship Channel in the north of the bay (mean depth ~12 m) and the shallower Sampan Channel in the south (mean depth ~6 m).

[8] Kaneohe Bay experiences mixed, dominantly semidiurnal tides with a mean tidal range of ~0.7 m and maximum range ~1.1 m. Annually, significant wave heights incident to Kaneohe Bay typically range from ~1 to ~4 m (Figure 2a) and are derived from two primary sources: (1) trade wind waves (periods 6–10 s) occurring throughout the year with significant wave heights ~1–3 m and (2) North Pacific ocean swells (periods 10–14 s) occurring during winter months, often with significant wave heights in excess of 3 m. Wind patterns in the Hawaiian Islands are dominated by the northeasterly trade winds (speeds typically 5–10 m/s) that are prevalent most of the time from May through October (Figure 2b). From October through April, trade winds still generally dominate, but occur less frequently.

2.2. Field Measurements

[9] An intensive field experiment measuring waves, currents and setup throughout Kaneohe Bay was conducted between January–March 2006 (Figure 1a). Details are given by *Lowe et al.* [2009] and are only summarized here. Wave conditions were measured hourly at seven locations on the forereef and reef flat (W1–W4 and A2–A4) using four Seabird Electronics 26 wave pressure gauges and the pressure sensors on three Acoustic Doppler Current Profilers (ADCPs) (Table 1). An additional pressure gauge was also deployed inside the central lagoon (W5) to sample variability in mean water level. Vertical profiles of 3D current velocities were measured hourly with ADCPs at seven locations (A1–A7) on the reef, within each channel and in the lagoon (Figure 1a). The spatial distribution of wave setup $\bar{\eta}$ was inferred from the pressure sensor data, defined relative to the mean water level on the forereef (located prior to wave breaking), where we assumed set down to be negligible (see *Lowe et al.* [2009] for details). Setup could only be estimated for instruments deployed on a hard reef platform (A2–A4 and W3–W5), since instru-

Table 1. Field Instrument Locations and Deployment Information

Site	Mean Depth (m)	Instrument	Conditions Measured
A1 (channel)	6.3	ADCP (1200kHz)	currents
A2 (reef flat)	2.0	ADCP (1200kHz)	currents, waves
A3 (reef flat)	2.0	ADCP (1200kHz)	currents, waves
A4 (reef flat)	5.1	ADCP (1200kHz)	currents, waves
A5 (channel)	11.4	ADCP (1200kHz)	currents
A6 (lagoon)	15.3	ADCP (600kHz)	currents
A7 (lagoon)	15.8	ADCP (600kHz)	currents
W1 (forereef)	8.1	SBE 26	waves
W2 (forereef)	7.9	SBE 26	waves
W3 (reef flat)	2.7	SBE 26	waves
W4 (reef flat)	2.5	SBE 26	waves
W5 (lagoon)	2.3	SBE 26	water level

ments deployed in the sand channels gradually sank by up to 5 cm over the experiment, making it difficult to identify an accurate reference level. Comparison between modeled and observed setup was conducted at subtidal frequencies by low-pass filtering the water level time series [*Beardsley et al.*, 1985], in order to isolate the much smaller setup variations (<0.1 m) from the dominant mean water level variability associated with the tides (tidal range ~1 m). Given its small magnitude, the percent uncertainties in measured setup (ranging from ~30–50% for all sites) [*Lowe et al.*, 2009], were much greater than the corresponding percent errors associated with measured wave heights and depth-averaged currents (both typically < 5%).

2.3. Model Description

[10] The 3D numerical model used for this study was Delft3D (WL|Delft Hydraulics). A detailed description of the model is given by, for example, *Lesser et al.* [2004], and is only summarized here. The Delft3D-FLOW module (version 3.55) simulates water motion due to surface wave, wind, tide, and buoyancy forcing. Flow is simulated by solving the unsteady shallow-water (hydrostatic) equations in three dimensions on a horizontal curvilinear Arakawa "C" grid and a vertical σ level (terrain-following) grid. The momentum and continuity equations are solved using the Alternating Direction Implicit method, subject to a prescribed set of initial and boundary conditions (discussed below).

[11] Sub-grid scale mixing of mass and momentum can be parameterized in Delft3D using a variety of turbulence closure schemes; for this study we employed a *k-L* scheme, which solved the turbulent kinetic energy equation, with dissipation modeled using an analytically prescribed mixing length L. The bed stress, τ_b, was modeled using a quadratic drag law based on the Eulerian velocity $\vec{u}_b$ in the grid cell just above the bed, i.e., $\vec{\tau}_b = \rho C_d |\vec{u}_b|\vec{u}_b$, where C_d is a bottom drag coefficient. C_d was related to a Nikuradse roughness length k_c based on a White-Colebrook friction formulation. The enhancement of near-bed turbulence and bed shear stresses by surface waves was modeled as a function of the ratio of the near-bed current to wave velocities using the formulation proposed by *Fredsoe* [1984]. Surface momentum fluxes generated by wind stresses were parameterized using a quadratic drag law based on the local wind velocity and an empirical drag coefficient [*Smith and Banke*, 1975]. Enhanced turbulence near the surface generated by breaking surface waves was also included following *Deigaard et al.* [1986; see also *Walstra et al.*, 2000], on the basis of the amount of local wave-breaking dissipation output from the numerical wave model.

[12] The transformation of random, short-crested surface waves was simulated using the third-generation SWAN wave model (version 40.51) [*Booij et al.*, 1999] incorporated into Delft3D. SWAN solves the spectral wave action balance equation on a horizontal curvilinear grid, accounting for the refraction and diffraction of wave energy, dissipation by bottom friction, depth-limited breaking and whitecapping, as well as wave generation by local winds. Given our relatively small domain, local wave generation should be of minor importance and hence was turned off in our model. The local rate of dissipation by depth-limited breaking S_b for each directional wave frequency component (σ, θ) was parameterized using the formulation of *Battjes and Janssen* [1978],

$$S_b(\sigma,\theta) = -\frac{1}{4}\alpha_{BJ} Q_b \left(\frac{\bar{\sigma}}{2\pi}\right) H_{\max}^2 \frac{E(\sigma,\theta)}{E_{tot}} \quad (1)$$

where $\alpha_{BJ} = 1$, Q_b is the fraction of breaking waves [*Booij et al.*, 1999], $\bar{\sigma}$ is the mean wave frequency, $H_{\max} = \gamma h$ is the local maximum stable wave height (expressed by the product of the local water depth h and an empirical breaker coefficient γ). Here $E(\sigma, \theta)$ is the wave energy spectrum and E_{tot} represents the total energy within the spectrum. Rates of bottom friction dissipation S_f for each wave component were parameterized using the spectral wave formulation proposed by *Madsen et al.* [1988], which was previously found by *Lowe et al.* [2005] to accurately characterize frictional dissipation rates across the Kaneohe Bay reef:

$$S_f(f,\theta) = -f_w \frac{U_{rms}\sigma^2}{\sqrt{2} g \sinh^2(kh)} E(\sigma,\theta) \quad (2)$$

Here, U_{rms} represents the root mean-squared near bottom wave velocity, k is the wave number, and f_w is a frequency-dependent wave friction factor, parameterized by the local ratio of the near-bottom wave excursion amplitude to a prescribed bed roughness length scale k_w, following *Jonsson* [1966].

[13] Finally, wave forcing provided by radiation stresses (e.g., due to breaking) was modeled following *Dingemans et al.* [1987], where contributions other than those due to the total wave dissipation (summed over all frequency components) are neglected [see also *Lesser et al.*, 2004]. Thus, the enhancement of wave forces by rollers inside the surf zone was not included in the present study. Wave forces output from SWAN were incorporated as additional stresses at the water surface in Delft3D, although theoretically these forces would have some vertical distribution through the water column [e.g., *Mellor*, 2003].

2.4. Model Domain and Configuration

[14] Separate orthogonal curvilinear grids were used to compute current and wavefields (Figure 3). Three-dimensional current fields were calculated on a 370 × 210 horizontal grid, with a resolution ranging from 40 m on

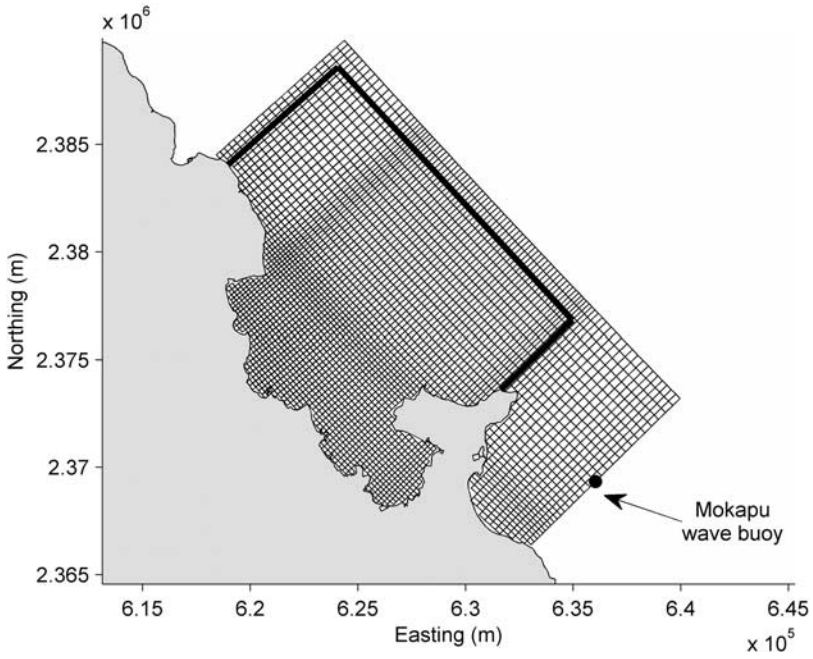

Figure 3. Computational grids. The wave model extends over the full domain shown, with the location of the directional wave buoy indicated. The circulation grid was nested within the larger wave grid, with its open boundaries denoted by the thick line. Note that because of the high spatial resolution, for visualization purposes the edges of only every 4 × 4 actual cells are shown.

the reef flat to as great as 90 m offshore. In the vertical, 10 σ levels were used, with the vertical spacing of the levels decreasing logarithmically toward both the surface and bottom of the water column. The circulation grid was nested within a larger wave grid (Figure 3). The same grid resolution was used over the region of grid overlap, but the wave grid was extended to the southeast so that its boundary coincided roughly with the location of a Datawell directional wave buoy located off Mokapu peninsula (21°25′ N, 157°41′ W), operated by the University of Hawaii Sea Level Center. The depth of each grid cell was interpolated from bathymetry data derived from two sources (Figure 1b): (1) very high resolution (~3 m horizontal resolution, 0.1 m vertical resolution) LIDAR bathymetry inside Kaneohe Bay (regions with depths <10 m), provided by the Army Corps of Engineers, and (2) a larger-scale National Ocean Service (NOS) bathymetry map (~60 m horizontal resolution) that was used everywhere else (e.g., for offshore regions). On the wave grid, directional wave spectra were simulated from 0–360 degrees, for wave frequencies ranging between 0.04 and 1.0 Hz, using 24 logarithmically distributed frequency bins and using a 6 degree directional resolution. During model simulations, SWAN was iteratively coupled to the Delft3D-FLOW module. Communication between the models occurred after a stationary wavefield was computed by SWAN (in our application once per hour), at which time wave information passed to Delft3D-FLOW was used to compute both mass transport by Stokes drift and wave forces due to radiation stress gradients.

[15] Wind forcing in the model (applied uniformly across the domain) was provided by direct measurement of wind speed and direction from a wind anemometer deployed on Kapapa Island, located at roughly the center of the bay. Tidal forcing was provided using the 20 dominant tidal constituents in Kaneohe Bay, inferred using data from a long-term water level station operated by NOAA (http://tidesonline.nos.noaa.gov), located inside Kaneohe Bay (21° 26.2′ N, 157° 47.6′ W). Evaluation of the tidal elevations at the various stations (forereef, reef flat and lagoon) during the *Lowe et al.* [2009] study indicated that there were no appreciable differences in both tidal amplitude and phase over this relatively small domain. Wave forcing was provided by data obtained from the offshore directional wave buoy, using the recorded significant wave height H_s, average period T_{m01}, mean wave direction D_m, and directional spreading θ_{sp}. For simplicity, these wave parameters were used to specify a parametric directional wave spectrum, assuming a JONSWAP temporal distribution with a default peak enhancement factor value of 3.3 and a cosine power directional distribution [*Booij et al.*, 1999].

[16] The same spatially constant, time-varying wave condition was prescribed along each of the three open wave boundaries (Figure 3); however, variations in wave height along each lateral boundary must occur as a result of their transformation in shallow water. Nonetheless, we found from preliminary simulations that setting wave heights to be constant along these boundaries had no significant effect on waves propagating within our smaller study region in Kaneohe Bay given its distance (several km) from the lateral boundaries of the much larger numerical domain. For the circulation model, a water level boundary condition was specified along the offshore boundary, as derived from the tidal harmonics. At each lateral (cross-shore) boundary, a Neumann (water level gradient) boundary condition was

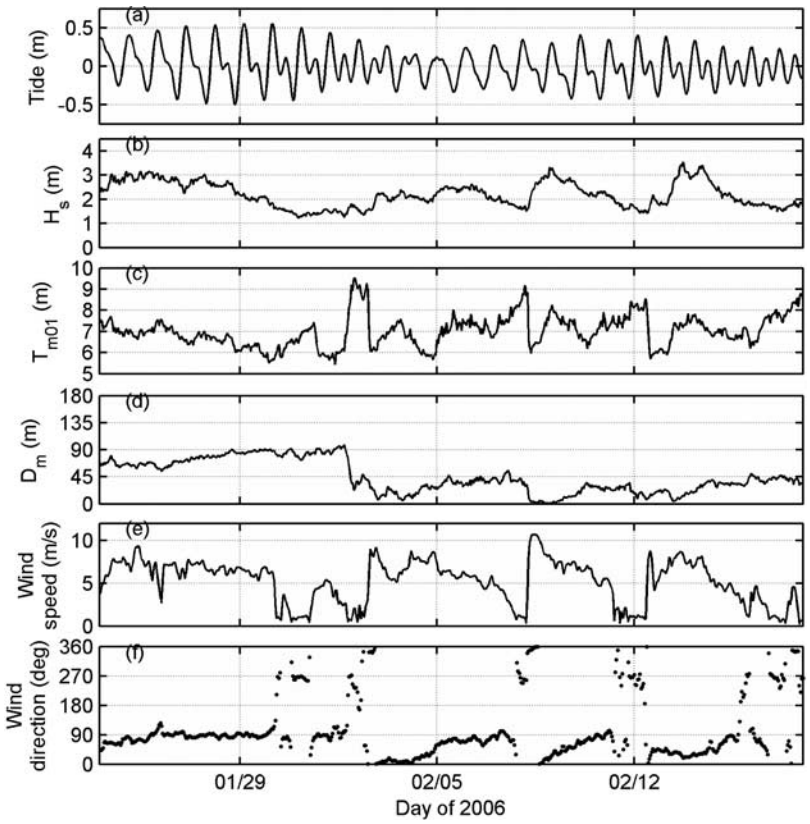

Figure 4. Physical forcing conditions used to drive the hindcast model simulations: (a) tidal elevation, (b) offshore significant wave height, (c) mean wave period, (d) mean offshore wave direction, (e) local wind speed, and (f) wind direction. Tidal elevation data were from the NOAA tide station maintained within Kaneohe Bay, wave parameters (H_s, T_{m01}, D_m) were derived from the offshore wave buoy, and wind parameters were derived from a wind anemometer deployed on Kapapa Island.

prescribed [*Roelvink and Walstra*, 2004]. For this application the water level gradient along these boundaries was set to zero, which permits flow to cross these boundaries but cannot account for the presence of any large-scale alongshore pressure gradients. Given the complexity of the regional ocean circulation around the Hawaiian Islands [e.g., *Alford et al.*, 2006], to incorporate these effects into the model would require nesting it within a much larger-scale ocean model, which was beyond the scope of the present study. However, we found from both field observations and initial model testing, that circulation in Kaneohe Bay (both on the reef flat and inside the lagoon) was very insensitive to any large-scale offshore currents [*Lowe et al.*, 2009]. This is not really surprising, since this nearshore circulation is primarily locally generated within the bay (e.g., by local surface waves) and given the negligible phase difference in the tides along the entrance of the bay due to its relatively short extent (~8 km); consequently, the tides would act approximately uniformly along the entrance to Kaneohe Bay to drain and fill the lagoon.

2.5. Model Validation and Application

[17] To quantify the ability of the model to predict waves, currents and setup in Kaneohe Bay, a hindcast simulation was conducted for a 4-week period (24 January to 18 February 2006; see Figure 4). To compare our model predictions of a given variable of interest X_{model} to our observations X_{obs}, a measure of "model skill" [*Warner et al.*, 2005], also referred to as the "index of agreement" [*Willmott et al.*, 1982], was computed as

$$\text{Skill} = 1 - \frac{\sum |X_{\text{model}} - X_{\text{obs}}|^2}{\sum \left(|X_{\text{model}} - \overline{X_{\text{obs}}}| + |X_{\text{obs}} - \overline{X_{\text{obs}}}| \right)^2}, \qquad (3)$$

in which the overbar denotes a time-averaged variable. Thus, perfect agreement between model output and observations at each site would yield a value of 1, while complete disagreement would yield a value of 0.

[18] We initially performed a wide range of simulations, in order to conduct a detailed investigation into the sensitivity of the model output to its various parameters. Sensitivity tests of the various parameters in SWAN confirmed that the wave breaker coefficient γ and the bottom roughness length k_w were the two dominant parameters controlling the spatial distribution of wave energy across the reef-lagoon system. Although wave dissipation on sandy beaches is typically dominated by breaking, given the large bottom roughness of coral reefs, dissipation by bottom friction can also be a significant (or even the dominant mechanism [see, e.g., *Lowe et al.*, 2005]). Thus, during our evaluation of the wave model, we initially investigated the influence of both γ and k_w by varying these parameters over

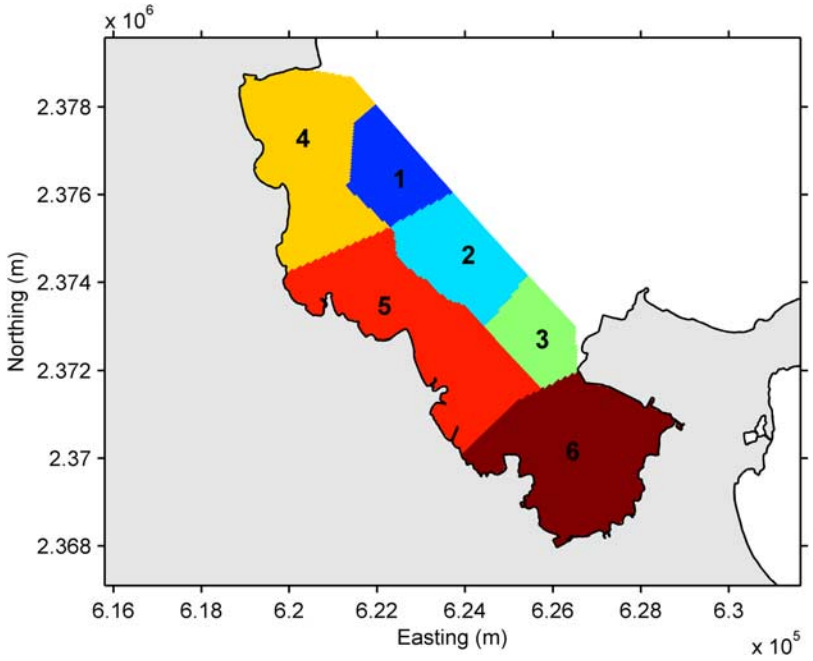

Figure 5. The six residence time zones defined for Kaneohe Bay.

a wide range of physically reasonable values (γ = 0.5–1.0, k_w = 0.01 – 1.0 m).

[19] A similar sensitivity analysis was also conducted for the circulation model, and it was concluded that the bottom roughness length scale k_c (assumed spatially uniform across the domain) was the dominant parameter influencing the results. For example, a comparison between 2D and 3D simulations, revealed minimal differences in currents generated on the shallow reef and in the channels, however, the 3D simulations agreed somewhat better with our observations at the much deeper lagoon sites (A6 and A7); as a consequence all simulations were conducted in 3D. Other tests conducted to examine the model sensitivity to the time step, grid resolution and number of σ layers revealed that reducing the resolution of the default values (1 min, ~40 m, and 10 layers, respectively) in half had no appreciable influence on the results. The results were also insensitive to horizontal eddy viscosities between 0.1 and 1 $m^2\ s^{-1}$, so we used a value ν_H = 0.4 $m^2\ s^{-1}$ based on the mean value measured from a dye and drifter dispersion study on the Kaneohe reef flat conducted by *Falter et al.* [2008]. Calibration of the circulation model, thus involved quantifying the model skill over a range of bottom roughness lengths (k_c = 0.01–1.0 m), subject to the wave forcing provided by the calibrated wave model.

[20] To investigate the role of various physical forcing mechanisms (waves, winds, and tides) on the circulation of Kaneohe Bay, the calibrated model was then forced with a variety of different wave, wind and tidal scenarios. We chose residence time as the best scalar parameter to quantify the importance of each mechanism in driving variations in reef circulation. For the present purposes we define "residence time" or "water export time" $T_{res}(x_0, y_0)$ [*Jouon et al.*, 2006; *Monsen et al.*, 2002], to be the time taken for a water parcel initially located inside Kaneohe Bay at position (x_0, y_0) to be transported out of bay (i.e., to mix with the open ocean). The calculation of residence times has an additional advantage in that it is also a key parameter used to estimate the rate at which biologically important material on the reef (e.g., nutrients and larvae) exchanges with the open ocean. T_{res} was calculated using a Lagrangian particle tracking algorithm [*van den Boogaard et al.*, 1993], which simulated the advection and dispersion of neutrally buoyant particles released throughout the domain. Advective transport was computed between time steps via numerical integration of the 3D current vectors output from the hydrodynamic model, which were interpolated to each particle location from the velocities available at the computational cell borders. Dispersion of the particles was modeled as a random walk process, using the vertical dispersion coefficients D_v output from the turbulence model and a spatially uniform horizontal dispersion coefficient D_h. Given that a horizontal dispersion coefficient D_h throughout Kaneohe Bay was not accurately known, we evaluated residence times for two cases, D_h = 0.2 $m^2\ s^{-1}$ and 2.0 $m^2\ s^{-1}$, on the basis of the range of values cited for other coral reefs [*Jones et al.*, 2008; *Spagnol et al.*, 2002] as well as measurements specifically on the Kaneohe reef flat (mean 0.4 $m^2\ s^{-1}$, range 0.2–1.0 $m^2\ s^{-1}$ [*Falter et al.*, 2008]). For each forcing condition, three particles were released in each grid cell throughout the bay (~40,000 particles total). The raw particle tracks were then postprocessed to determine the time when each particle crossed the Kaneohe Bay boundary (Figure 5), thus enabling spatial maps of T_{res} for each forcing condition to be calculated. Residence times were also defined for each of the six zones defined in Figure 5, by computing the average residence time of grid cells comprising each zone, weighted by cell volume [*Jouon et al.*, 2006]. Although particles leaving the bay could reenter the bay from offshore at a later time because of recirculation, given that the large-scale regional currents surrounding the Hawaiian Islands (not modeled in the present study) would

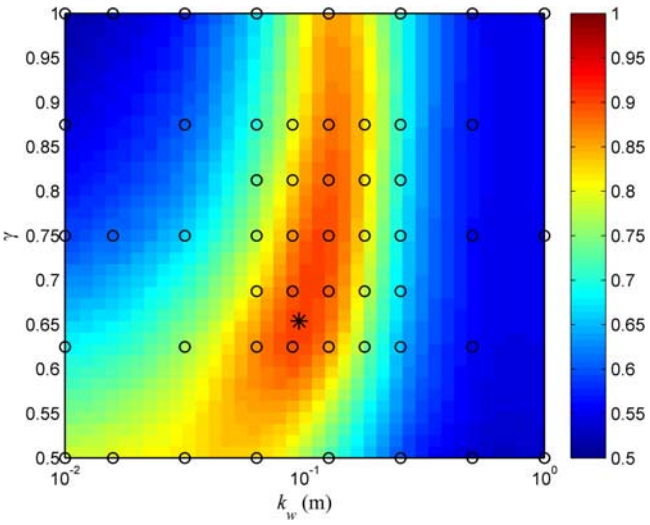

Figure 6. Model skill for significant wave height, representing the average value for all 7 wave measurement locations, as a function of γ and k_w (each circle denotes an individual simulation). The asterisk denotes the point with maximum skill 0.92 occurring at $\gamma = 0.64$ and $k_w = 0.09$ m.

drive particle transport in offshore waters, for simplicity we assume that a particle is "lost" when it first exits the bay. Given that the particle export time may also be sensitive to the phase of the tides in which the particles are initially released [*Monsen et al.*, 2002], for each forcing condition a total of four particle tracking simulations were conducted where particles were released on four different phases of the M2 tide: 0°, 90°, 180°, and 270° corresponding to peak high, ebbing, peak low, and flooding (~160,000 particles were thus released in total for each forcing). All reported residence times represent the average value predicted from each subset of the four tidal phase simulations.

3. Hindcast Model Results

3.1. Waves

[21] Application of SWAN using various (spatially uniform) values of γ and k_w, indicated that the values $\gamma = 0.64$ and $k_w = 0.09$ m best replicated the observed wave heights at the 7 wave measurement locations (Figure 6), with a site-averaged model skill of ~0.92 [equation (3)]. Moreover, for these values of γ and k_w, wave heights were accurately predicted at each individual site (Table 2), with skills ranging between 0.81 and 0.96. Inspection of the wave height time series at the various sites, confirmed that the wave model with $\gamma = 0.64$ and $k_w = 0.09$ m correctly predicted the wave height response on the forereef to changing offshore wave conditions, as well as the strong tidal modulation of wave heights observed at the reef flat and back reef sites (Figure 7).

3.2. Circulation

[22] For each model simulation, two values of skill were calculated: one representing the skill calculated exactly as in equation (3), using the current time series projected along the principal major axes derived from the field data, and a separate skill value calculated with the net (time-averaged) current removed from each time series. The latter provides additional evaluation of how well the model responds to variations in the physical forcing alone. The magnitudes of the time-averaged currents were generally of the same magnitude as the current variability (Table 3). Evaluation of the site-averaged (A1–A7) skills as a function of k_c indicated that the overall skill improved slightly with increasing k_c up to $k_c = 1.0$ m (Figure 8), although there was little difference between $k_c = 0.5$–1.0 (skills 0.65 versus 0.67). Comparison of skills calculated with net currents removed (Figure 8), indicate that the model best reproduced the current variability with a somewhat smaller value $k_c = 0.2$–0.5 m (site average skill ~0.90). On the basis of this analysis, it appears that a value $k_c = 0.5$ m provides a good balance between accurately modeling both the net current magnitudes and the current variability induced by changing wave, wind and tidal forcing. As a result, all simulations that follow use $k_c = 0.5$ m; for this value, model skill values are reported for each site (Table 3).

[23] Modeled and observed net (time-averaged) current vectors and velocity variance ellipses (Figures 9a and 9b) reveal that the model captures the dominant circulation and its variability throughout the system. The model does tend to slightly overpredict the net currents (by ~30%) at the deeper channel sites (i.e., A1, A5, and A7), which in large part accounts for the discrepancies between the two skill values reported for these sites (Table 3). A harmonic analysis of the modeled and observed current time series, processed using the Matlab toolbox T_TIDE [*Pawlowicz et al.*, 2002], indicates the model reproduces most of the observed tidal current variability, with tidal ellipses for the dominant M2 component shown in Figure 9c. The model thus confirms *Lowe et al.*'s [2009] observations that tidal currents are roughly 2–4 times stronger through the deeper channels compared to over the shallow reef flat, and also somewhat stronger inside the shallower Sampan Channel than in the Ship Channel (Table 3). Direct inspection of the current time series along the principal major axes with net currents removed, shows that the model, in general, accurately reproduces both the tidal and subtidal variability observed at all sites (Figure 10), albeit with a slight underprediction of the tidal response at channel site A1 and the subtidal response at the reef site A3.

3.3. Wave Setup

[24] Low-pass-filtered (subtidal) wave setup fields output from the model were compared to corresponding field measurements described by *Lowe et al.* [2009] (Figure 11). Modeled setup is in fair agreement with observations on the

Table 2. Comparison Between Field Observations and Model Output for Wave Heights

	H_s (m) (Mean SD)		
Site	Field	Model	Skill
W1	1.69 (0.44)	1.67 (0.40)	0.96
W2	1.54 (0.38)	1.60 (0.37)	0.96
A2	0.57 (0.08)	0.56 (0.09)	0.93
A3	0.61 (0.08)	0.60 (0.09)	0.94
A4	0.84 (0.14)	0.90 (0.11)	0.81
W3	0.47 (0.10)	0.50 (0.09)	0.93
W4	0.61 (0.11)	0.60 (0.10)	0.89

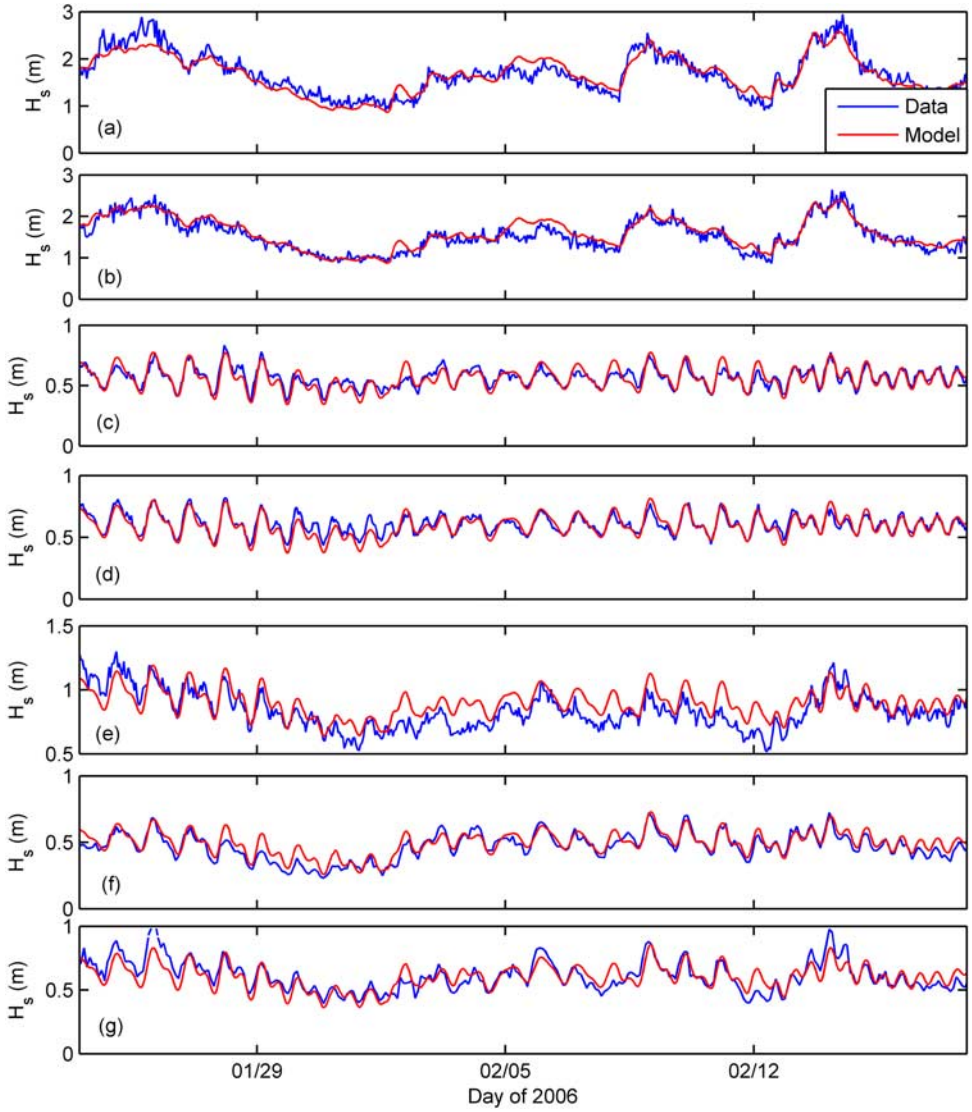

Figure 7. Comparison between observed and modeled significant wave height time series for $\gamma = 0.64$ and $k_w = 0.09$ m, as measured on the forereef (a) W1 and (b) W2, on the reef flat at (c) A2, (d) A3, and (e) A4, and on the back reef at (f) W3 and (g) W4.

reef flat (A2) and within the lagoon (W5), with skill values 0.79 and 0.61, respectively (Figures 11a and 11b). On average, the model does appear to slightly overpredict setup at both sites by ~1–2 cm, however, model results are generally in good agreement with observations to within the uncertainty of the measurements. For the remaining sites where setup was measured (i.e., A3–A4 and W3–W4), skill values were similar (ranging from 0.55 to 0.76). A

Table 3. Comparison Between Observed and Modeled Depth-Averaged Currents[a]

	Net Current Magnitude		Net Current Direction		Current Variability (Standard Deviation)		M2 Tidal Current Amplitude			
Site	Field	Model	Field	Model	Field	Model	Field	Model	Skill	Skill (Offset Removed)
A1	10.1	13.1	40	49	10.2	6.0	7.1	5.0	0.64	0.87
A2	8.0	11.3	240	233	6.1	5.1	2.0	2.7	0.67	0.92
A3	16.3	15.9	276	261	8.3	4.2	1.9	2.1	0.68	0.95
A4	4.2	8.9	353	3	3.7	4.5	2.2	3.9	0.44	0.92
A5	9.3	14.5	47	51	9.3	6.5	3.7	4.0	0.63	0.90
A6	0.0	1.0	25	324	4.4	3.1	3.5	2.7	0.84	0.86
A7	3.2	7.3	2	350	7.0	6.8	3.6	4.9	0.74	0.89

[a]Currents are in units of m s^{-1}.

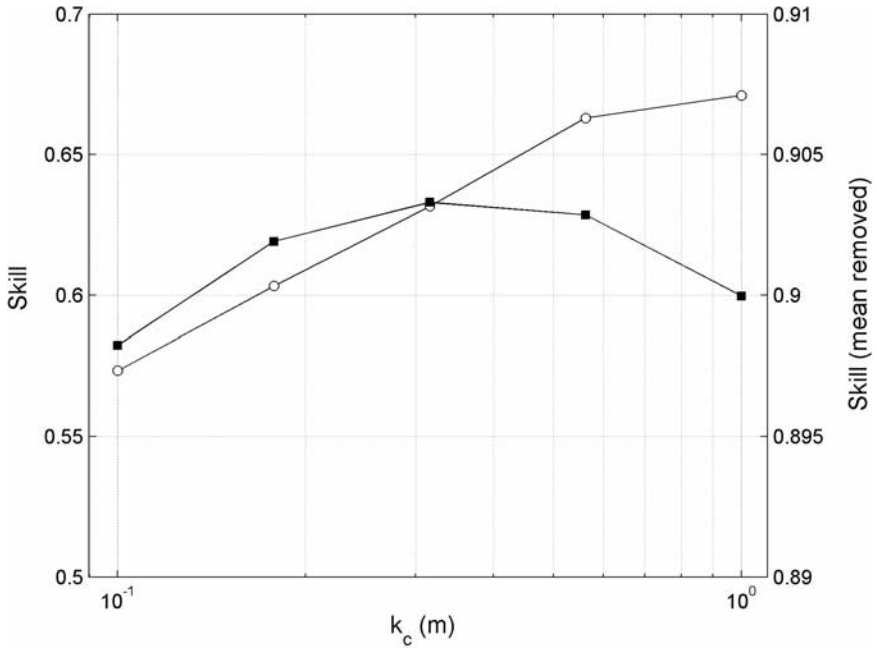

Figure 8. Model skill values for currents as a function of bottom roughness length k_c, averaged over all sites. Open circles indicate skill calculated directly from equation (3). Closed circles indicate skill with time-averaged current speeds removed.

spatial map of the time-averaged setup field during the simulation period (Figure 11c), revealed a region of elevated mean water level (~7 cm) over the shallow reef flat near the center of the bay, with lower setup values (~3–4 cm) throughout the lagoon and the deeper reef sections.

4. Reef-Lagoon Residence Times and Sensitivity to Physical Forcing

[25] A series of numerical experiments were conducted using the calibrated model, to investigate how wave, wind and tidal forcing control the spatial distribution of residence times within Kaneohe Bay. A total of 11 forcing conditions were considered (P1–P11, Table 4), with the particular conditions chosen on the basis of the range observed from historical observations. Analysis of wave and wind data over the 2 year period 2005–2006 (Figure 2), indicate significant wave heights generally ranged between 1 to 4 m (mean ~2 m) while winds ranged between 2 and 10 m/s (mean ~5 m/s). Both wave and wind directions are dominantly from ~75 degrees, however, may vary from ~165 to 345 degrees. It is not possible to simulate all possible forcing scenarios, so to limit our number of particle tracking runs, we start with a default set of conditions based on mean values from each forcing time series. For each run, we thus focus on a single forcing mechanism (tide, wave, or wind) and then perturb its value away from the mean set of conditions. Our base forcing condition (run P1) in Table 4, is chosen to have a representative M2 tidal range of 0.7 m (denoted T_o), a significant wave height 2 m from 75 degrees (denoted WV_o), and a wind speed of 5 m/s from 75 degrees (denoted WD_o). Subsequent runs were selected to quantify differences in residence times resulting from neap (0.4 m) and spring (1.0 m) variability in tidal ranges, small (1.0 m) and large (4.0 m) incident waves, and weak (2 m/s) and strong (10 m/s) wind speeds. Additional runs were also conducted to investigate the role of changing wave and wind directions.

[26] A residence time map for the default forcing condition (run P1) reveals a high degree of spatial heterogeneity across the system (Figure 12). Residence times in the northern region of the bay (zones 1 and 4; see Table 4) are relatively fast at ~1 day. In stark contrast, residence times in the southern bay (zone 6) are extremely slow (1–2 months), indicating that this region is only weakly connected to the open ocean. Interestingly, residence times are somewhat large for the central reef flat (zone 2; ~6 days) despite its shallow depth (Figure 1b). From these simulations, it is apparent that material in this region becomes advected across the reef flat and becomes entrained into much more sluggish lagoon waters of zone 5. Furthermore, throughout most of the system (zones 1–5) there are only minor differences in residence times between simulations with D_h = 0.2 m^2 s^{-1} and 2.0 m^2 s^{-1}, ±5–10% typically, indicating that transport in these regions is dominated by advection. However, predicted residence times in the southern lagoon (zone 6), are strongly influenced by D_h because of sluggish advection (i.e., a ~30% change for run P1).

[27] Results for the full range of forcing conditions simulated in Table 4 reveal that, across most of the system (zones 1–2; 4–5), there are only minor differences in residence times between neap (run P2) and spring tide (run P3) conditions. A major exception is the southern lagoon (zone 6), where a spring tide can result in an ~30–40% reduction in residence time. Tides also moderately influence residence times in zone 3; while this includes the shallow (~5 m) Sampan Channel where flows are dominantly wave-driven, this zone also includes regions

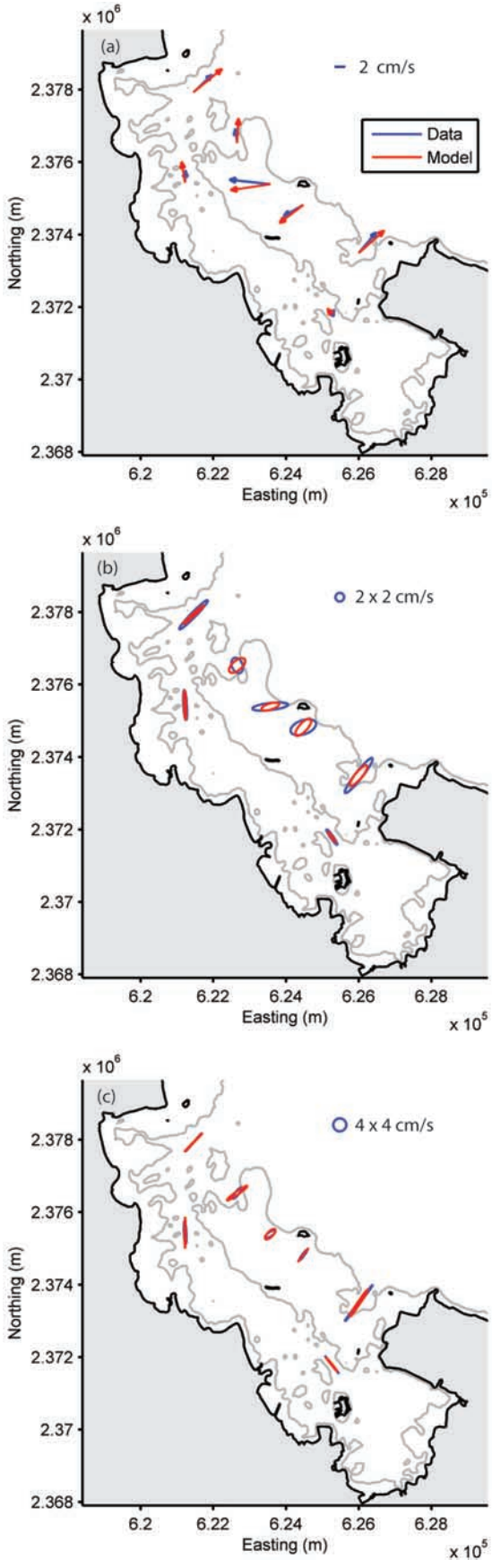

Figure 9. Field observations and model results of (a) net (time-averaged) current vectors, (b) velocity variance ellipses, and (c) tidal ellipses for the M2 component. Note the differences in the velocity scales. The 4 m bathymetry contour is superimposed as a gray line.

of deeper (>10 m) lagoon water that would be expected to significantly impact the volume weighted residence times.

[28] In contrast, increasing incident wave forcing (runs P4 versus P5) significantly reduces the residence times over most of the system (zones 1–5). However, increasing offshore significant wave heights by a factor of four only reduces residence times in the southern bay (zone 6) by ~20%, thus reinforcing the notion that this region is largely isolated from the relatively strong wave-driven flows generated over the reef. While varying wind speeds (runs P6 and P7), have only a minimal effect on residence times in the shallow reef regions (zones 1–4) where flows are primarily wave-driven, winds appear to play an important role in flushing the deep lagoon (zones 5 and 6). In particular, under strong wind conditions (10 m/s), residence times in the southern bay are reduced by ~30–50%.

[29] Finally, simulations conducted for different offshore wave directions (runs P8 and P9), indicate that residence times throughout Kaneohe Bay can decrease significantly as the wave direction varies from southerly (Θ_{WV} = 165°) to northerly (Θ_{WV} = 345°). Because of geographic orientation and the presence of Mokapu peninsula, Kaneohe Bay is largely sheltered from southerly swells. The effect of varying wind direction is generally much less pronounced, however, both a southerly (Θ_{WD} = 165°) and northerly (Θ_{WV} = 345°) wind produce a lower residence time in the southern lagoon (zone 6), than for the dominant (default) onshore wind direction of Θ_{WD} = 75°. It appears that exchange with the southern lagoon is enhanced when the wind direction is aligned with the northwest-southeast orientation of the entrance channels to the southern lagoon (Figure 1).

5. Discussion

5.1. Model Performance

[30] The wave model performed remarkably well across the entire domain using spatially uniform values of γ = 0.64 and k_w = 0.09 m. This value of γ is in fact very similar to the default value γ = 0.73 in SWAN, based on a review of experimental data by *Battjes and Stive* [1985], while the value of k_w = 0.09 m is comparable to the k_w = 0.16 ± 0.03 m that *Lowe et al.* [2005] empirically found best parameterized frictional dissipation across a section of the Kaneohe reef flat. On the reef flat (A2) where the near-bed RMS wave orbital velocity is typically ~0.4 m/s, a value k_w = 0.09 m translates into a wave friction factor $f_w \sim 0.2$ [*Madsen et al.*, 1988], which is similar to the f_w = 0.28 ± 0.04 m measured on this reef flat [*Lowe et al.*, 2005]. We emphasize that the composition of the benthos does vary markedly throughout Kaneohe Bay, with reef substrate dominating both the forereef and majority of the reef flat region, while extensive sections of sand dominate the channel regions and the large sandbar located on the back of the reef flat (see Figure 1a). Nevertheless, the incorpo-

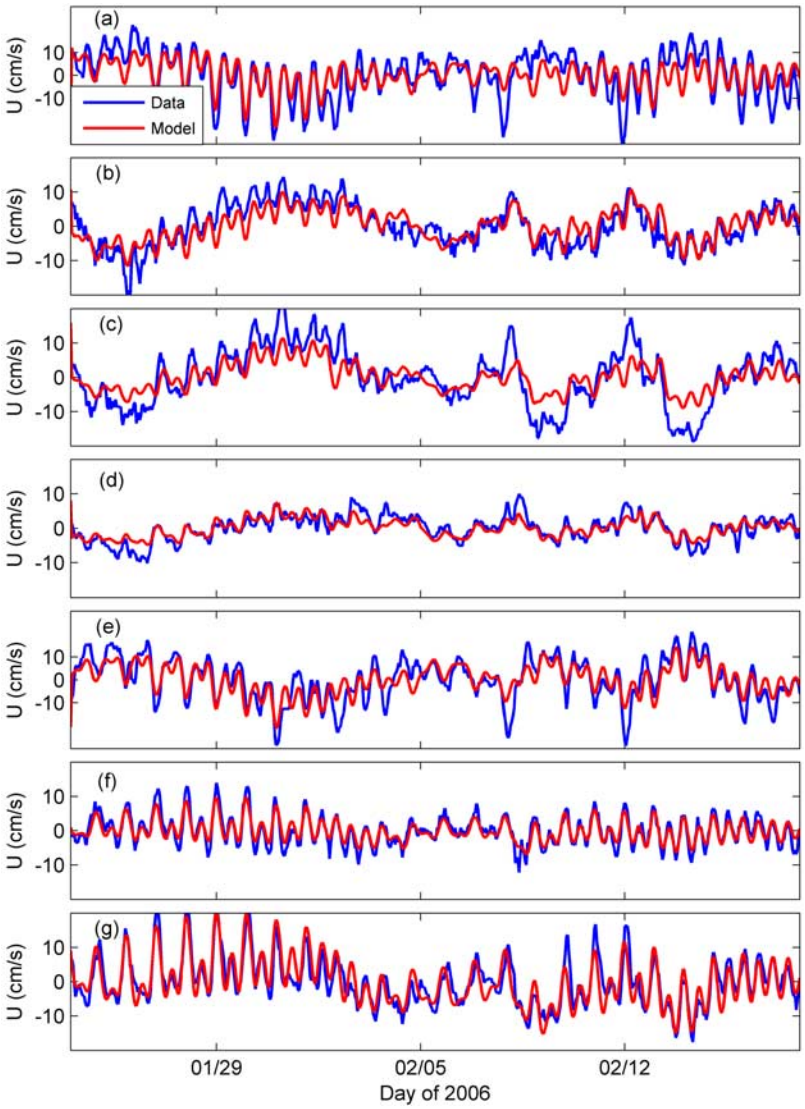

Figure 10. Comparison of time series variability in depth-averaged currents with net currents removed (projected along the field data principal major axis) for field observations and model output. Figures 10a–10g correspond to sites A1–A7, respectively.

ration of a spatially varying roughness map into SWAN does not appear to be necessary to accurately model the distribution of frictional wave dissipation (and hence overall wave transformation) within this particular reef system. This may be due to the fact that variations in wave friction factors controlling frictional dissipation are only influenced by order of magnitude changes in k_w. As a consequence, such spatial variations in physical roughness may not ultimately translate into large changes in wave friction factors; for example, k_ws for sandy beds with vortex ripples typically range between 0.01 and 0.10 m [*Nielsen*, 1992], thus still of the same order of magnitude as previous measurements of k_w on the Kaneohe reef by *Lowe et al.* [2005].

[31] The coupled circulation model applied using a spatially uniform k_c = 0.5 m also predicted the dominant circulation patterns throughout the system fairly accurately, including both its tidal and subtidal variability. On the reef flat where depths are ~1–2 m, a value k_c = 0.5 m corresponds to a quadratic current drag coefficient $C_D \sim 0.01–0.02$ (defined on the basis of a depth-averaged velocity and assuming a logarithmic velocity profile). This is similar to direct field estimates of $C_D \sim 0.02$ reported for the Kaneohe reef flat [*Lowe et al.*, 2009] and other C_D values reported in the literature for reefs ($C_{D,r} \approx 0.01–0.05$) [*Lugo-Fernandez et al.*, 1998; *Jones et al.*, 2008; *Hench et al.*, 2008; *Lowe et al.*, 2008]. The model matches field observations by *Lowe et al.* [2009] that the spatial distribution of wave energy on the reef (Figure 13a) dominantly generates onshore wave-driven flows over the shallow central region of the reef flat, with relatively strong return flows out each channel (Figure 13b). The success of the circulation model thus raises questions about how the use of a spatially uniform bottom roughness could be appropriate in a system that displays such a broad range of bottom types (see Figure 1a). In particular, this would suggest that the roughness experienced by currents over the reef (covered primarily by macroalgae with some limited coral) may

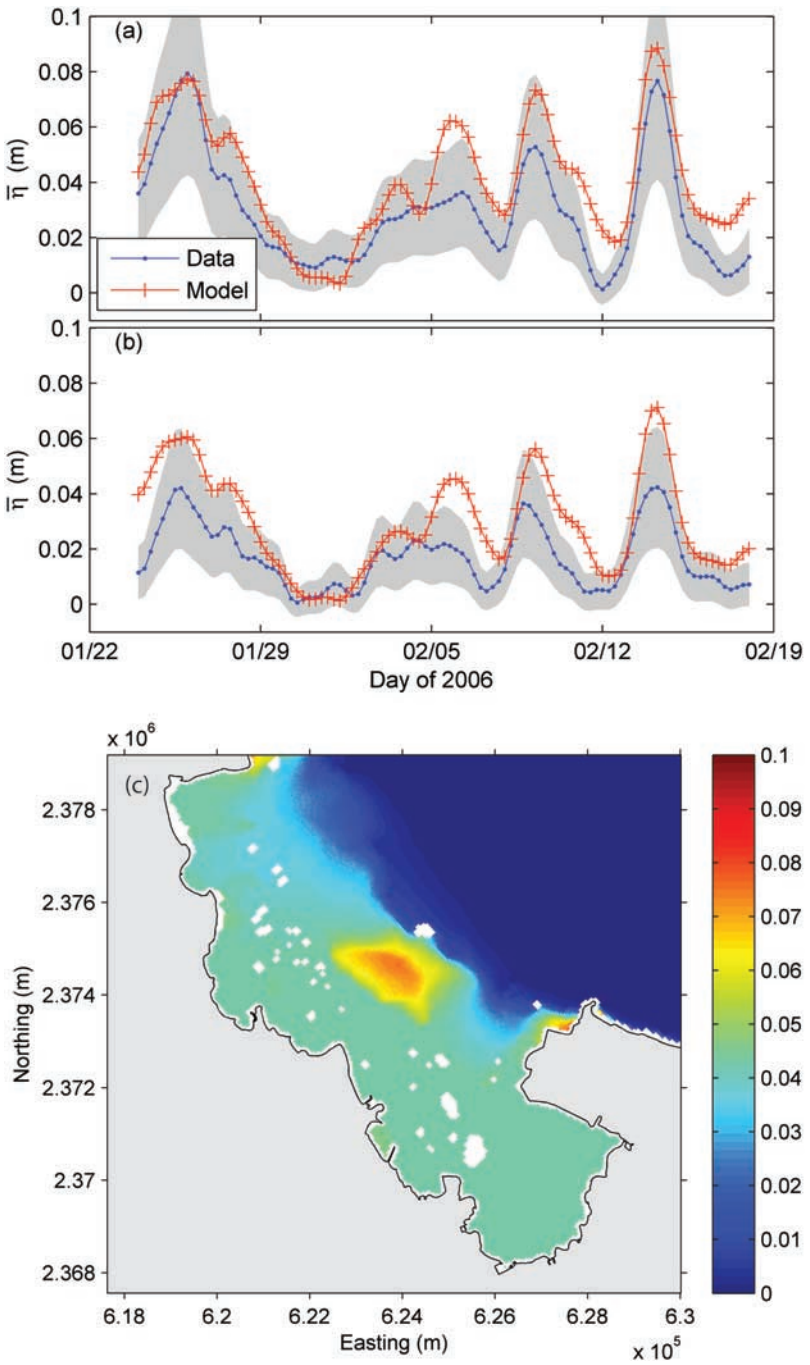

Figure 11. Comparison between field data and modeled wave setup (a) on the reef flat at site A2 and (b) in the lagoon at site W5. Gray regions denote the 95% confidence intervals in measured setup. (c) Modeled wave setup field $\overline{\eta}$ (in meters) under mean wave forcing (H_s = 2 m and T_p = 9 s).

effectively be comparable to the roughness associated with the lagoon (whose bottom consists largely of mud) and the channels (whose bottoms consist largely of sand). A number of explanations are possible. First, much of the lagoon bottom is populated with craters and mounds (~10–20 cm high) formed by burrowing shrimp and worms [*Jokiel*, 2008]. Second, current and wave action on the channel bottoms often form sand ripples 5–20 cm high (J. Falter, personal communication, 2008). Third, and probably most significant, both lagoon and channels are interspersed with numerous roughness features ranging from coral/limestone outcrops (several meters in diameter) to fully formed patch reefs (tens of meters) making the movement of water through these regions somewhat tortuous and rough (see Figure 1a). Such patches of roughness (many of which have diameters smaller than a single grid cell) have been shown to locally increase effective drag coefficients in their vicinity to order 1 or larger [*Reidenbach et al.*, 2006; *Monismith*, 2007] thus significantly augmenting the spatially integrated bottom drag beyond that associated with a purely flat sandy bed.

Table 4. Residence Times Under Idealized Forcing Conditions for Each Zone in Figure 5[a]

Run	Tide (m)	H_s (m)	U_{wind} (m/s)	Direction (degrees)	Residence Time (days), Zone 1	2	3	4	5	6
P1	T_o	WV_o	WD_o	-	**1.0** (*0.1*)	**6.2** (*0.2*)	**3.0** (*0.5*)	**0.8** (*0.1*)	**11.4** (*0.0*)	**41.9** (*11.5*)
P2	0.4	WV_o	WD_o	-	**1.0** (*0.1*)	**5.5** (*0.2*)	**5.3** (*1.3*)	**0.8** (*0.0*)	**12.0** (*0.9*)	**49.2** (*15.1*)
P3	1.0	WV_o	WD_o	-	**1.2** (*0.1*)	**6.3** (*0.0*)	**3.3** (*0.2*)	**1.0** (*0.0*)	**12.3** (*0.8*)	**34.3** (*8.8*)
P4	T_o	1.0	WD_o	-	**1.5** (*0.2*)	**10.0** (*0.2*)	**6.5** (*0.7*)	**1.3** (*0.1*)	**19.6** (*1.7*)	**46.9** (*12.4*)
P5	T_o	4.0	WD_o	-	**0.7** (*0.0*)	**4.3** (*0.2*)	**4.0** (*0.5*)	**0.7** (*0.0*)	**9.5** (*0.7*)	**38.8** (*9.8*)
P6	T_o	WV_o	2	-	**1.3** (*0.1*)	**6.3** (*0.6*)	**3.1** (*0.2*)	**1.1** (*0.0*)	**13.9** (*0.9*)	**43.9** (*6.4*)
P7	T_o	WV_o	10	-	**0.7** (*0.1*)	**5.1** (*0.2*)	**2.8** (*0.2*)	**0.7** (*0.0*)	**9.5** (*0.9*)	**23.3** (*5.2*)
P8	T_o	WV_o	WD_o	Θ_{WV} = 165°	**6.7** (*0.8*)	**18.7** (*0.9*)	**7.0** (*0.1*)	**5.6** (*0.4*)	**24.8** (*0.7*)	**41.8** (*9.7*)
P9	T_o	WV_o	WD_o	Θ_{WV} = 345°	**0.5** (*0.0*)	**2.2** (*0.1*)	**6.9** (*0.2*)	**0.8** (*0.1*)	**3.5** (*0.3*)	**33.6** (*6.4*)
P10	T_o	WV_o	WD_o	Θ_{WD} = 165°	**1.2** (*0.1*)	**6.4** (*0.0*)	**2.6** (*0.2*)	**0.9** (*0.0*)	**8.6** (*0.1*)	**23.3** (*4.5*)
P11	T_o	WV_o	WD_o	Θ_{WD} = 345°	**1.3** (*0.1*)	**5.8** (*0.1*)	**4.1** (*0.4*)	**1.2** (*0.0*)	**9.6** (*0.1*)	**20.9** (*2.5*)

[a]See text for details. Bold values denote mean residence times calculated for D_h = 0.2 m^2 s^{-1} and 2.0 m^2 s^{-1}. Italicized values in parentheses represent the average difference (±) from the mean residence time, as inferred from the two D_h computations.

[32] Despite the good overall agreement between modeled and observed currents (model skill >0.5 at all sites), the model did tend to predict slightly larger net currents (by ~30%) out each channel (A1 and A5). Such agreement at these sites could be improved by increasing k_c in the model; however doing so would then lead to poorer agreement at the reef flat sites (A2 and A3). Therefore, it is not clear whether the origin of this small discrepancy resides with the reef flat, channels, or both and ultimately could result from a number of factors including (1) inaccuracies in the bathymetry data, (2) spatial variability in bottom roughness, (3) deficiencies in modeled wave forces and the wave enhancement of bottom friction, and (4) sub-grid scale (<40 m) variations in flow patterns that are known to be present on reefs, for example, channelization of flow through bottom topography, etc. Considering the first factor, although this LIDAR-derived bathymetry data set represents one of the most accurate available for a coral reef, some data gaps exist inside the surf zone (where optical sampling is precluded) and also within any regions of the lagoon and channels that are too deep to sample (>10 m). For these regions, the model bathymetry was instead interpolated from much less accurate and sparse historical sounding data (see section 2.4); on the basis of mass conservation alone, a percent error in local depth would induce a proportional error in the local depth-averaged current. Considering the fourth factor, our current measurements were collected at only fixed points while our grid resolution by default averages over ~40 m, therefore, some discrepancy between the time series should be expected. These and other complicating factors will always pose challenges to rigorously vet model performance from a finite number of field observations alone.

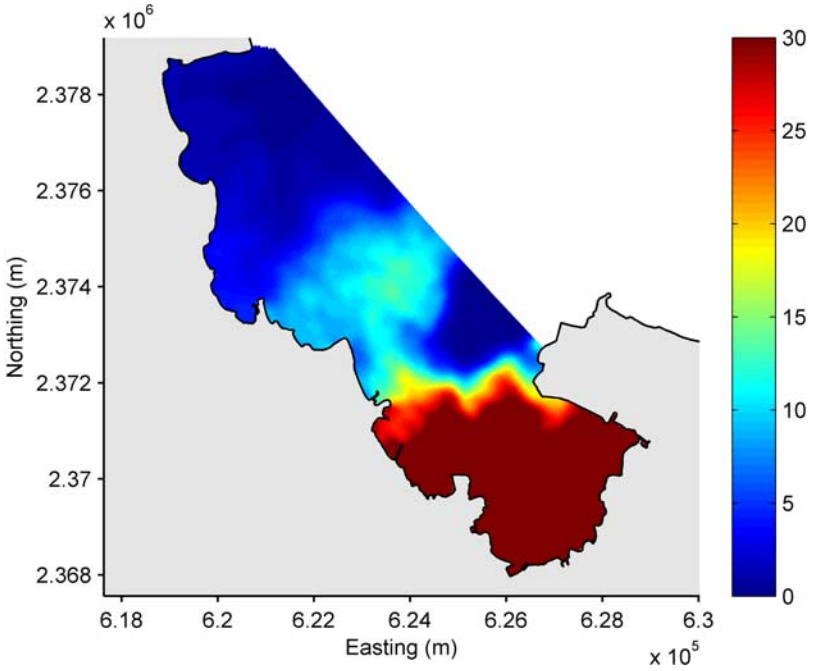

Figure 12. Residence time distribution (in days) for run P1, forced by the average historical wave, wind and tidal forcing. Results reflect the average residence times for the two D_h simulations (0.2 and 2.0 m^2 s^{-1}). Note that any residence times greater than 30 days are plotted as 30 days.

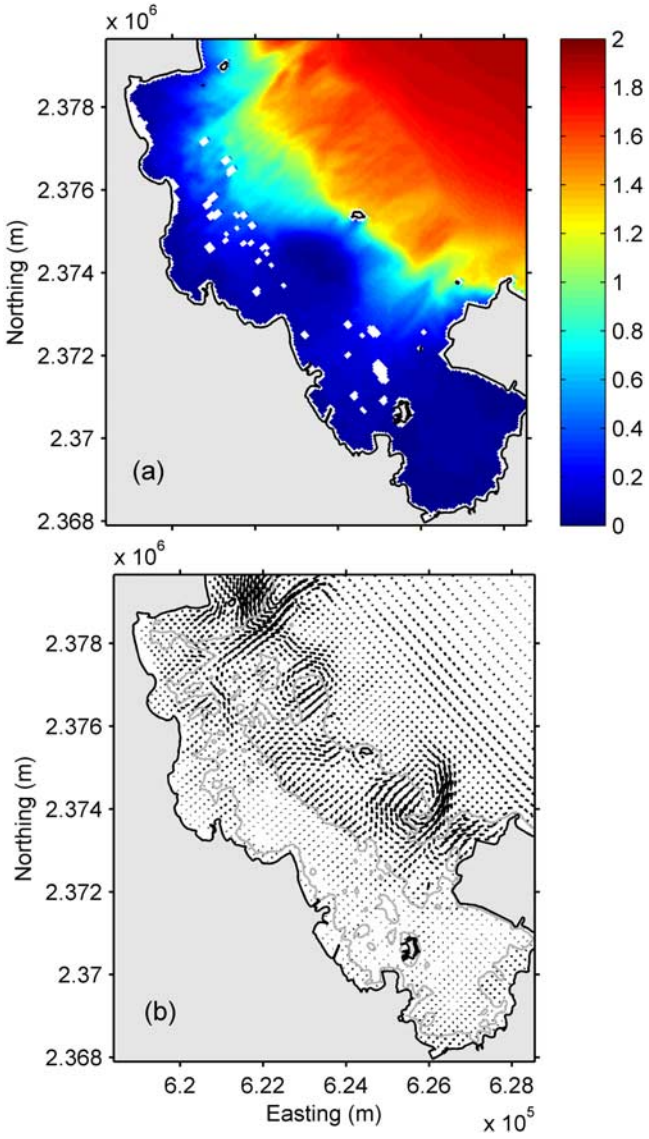

Figure 13. (a) Significant wave height distribution (in meters) forced by the mean offshore wave condition (H_s = 2 m, T_p = 9 s, Θ_{WV} = 75 degrees). (b) Corresponding depth-averaged current vectors (quasi-steady) driven by the wavefield in Figure 13a and a mean wind (U_{wind} = 5 m/s, Θ_{WD} = 75 degrees) condition, with the 4 m depth contour (in gray) included. Note that only one of every four vectors is shown.

[33] It was also apparent from Figure 10 that the model predicted a somewhat weaker circulation response to incident wave forcing variability over the reef flat, especially at A3. This behavior could be due to the wave-current interaction model overpredicting wave enhancement of bed shear stresses. Given that setup gradients driving these flows increase proportional to the incident wave energy flux in accordance with theory ($\sim H_0^2$) [*Lowe et al.*, 2009], the relationship between current speeds and incident wave height will ultimately depend on the formulation of the drag law that is used (i.e., linear versus quadratic). In the absence of near-bottom wave velocities U_w, the model assumes a quadratic drag law holds, in which case we would expect the magnitude U_c of the wave-driven currents to increase as $U_c \sim H_0$. However, as local wave velocities U_w increase relative to U_c, the drag formulation [*Fredsoe*, 1984] will transition from scaling quadratically with U_c, instead to linearly. In the limit as $U_w \gg U_c$, we would expect $U_c \sim H_0^{1/2}$. As a consequence, the weaker response of the modeled wave-driven currents in this system could, to some degree, be due to the effects of waves on modeled current bed stresses not being accurately parameterized.

5.2. Dominant Circulation

[34] The modeled 2D time-averaged current vector field over simulation period shows that two persistent circulation cells develop around the Ship and Sampan channels, with smaller circulation cells apparent near the surf zone because of localized variability in wave setup gradients (Figure 13). The model, furthermore, confirms field observations that the relatively strong net currents over the shallow reef flat do not generate strong wave-driven flows within the back lagoon (Figure 13); this is largely due to the large discrepancy in water depth between the reef flat and lagoon ($\sim$2 m versus $\sim$15 m). Nonetheless, the particle tracking results indicate that wave forcing does play an important role in flushing the northern lagoon (zone 4), and to some extent the central lagoon (zone 5). Wave forcing, however, clearly plays a minor role in flushing the southern lagoon, because of this region's being largely enclosed by Mokapu peninsula, and also given that it is only free to exchange with the rest of the system through two narrow channels on either side of Coconut Island (Figure 1).

[35] Clearly the inherently 2D circulation inside this coastally bounded reef-lagoon system is more complex than the roughly 1D cross-reef flows generated on many atolls and barrier reefs having deep, expansive lagoons [e.g., *Symonds et al.*, 1995]. This raises questions about the appropriateness of using existing 1D analytical models of wave-driven reef circulation to predict flows in entire coastal reef systems such as Kaneohe Bay, despite the fact that these models have been successfully applied to describe flows in smaller sections of reefs. Notably, all of these 1D models have assumed that wave setup inside the lagoon is zero, since these models assume the lagoon can freely exchange with the open ocean, i.e., as would be a reasonable assumption for many, but not all, atolls and barrier reefs. Both field observations and output from the 2D model (Figure 11) clearly show that setup inside the coastal lagoon is significant, and is a rather large fraction ($\sim$50–70%) of the maximum reef setup. This lagoon setup serves to decrease the cross-reef water level gradient responsible for driving these wave-driven flows. *Lowe et al.* [2009] presented a modified 1D model based on the general cross-reef momentum equations to estimate this lagoon setup, which considered the additional momentum dynamics of the lagoon-channel return flow. The application of this modified 1D model considering lagoon setup was able to reproduce wave-driven currents generated over the reef flat much more accurately. Nevertheless, applying a much more sophisticated 2D coupled wave-circulation numerical model to coastal reef-lagoon systems, as in this study, offers a number of advantages; namely, (1) they incorporate both

Table 5. Residence Time Sensitivity to Physical Forcing From Equation (4) for Each Zone in Figure 5 Calculated From the Mean Residence Times in Table 4[a]

	Zone 1	Zone 2	Zone 3	Zone 4	Zone 5	Zone 6
Tide, $\frac{\sigma_a}{T_{res,0}}\frac{\partial T_{res}}{\partial a}$	0.06	0.04	**−0.18**	0.09	0.01	**−0.13**
Wave, $\frac{\sigma_{H_s}}{T_{res,0}}\frac{\partial T_{res}}{\partial H_s}$	**−0.15**	**−0.17**	−0.15	**−0.14**	**−0.16**	−0.03
Wind, $\frac{\sigma_{U_{wind}}}{T_{res,0}}\frac{\partial T_{res}}{\partial U_{wind}}$	−0.10	−0.04	−0.02	−0.09	−0.07	−0.09

[a]Values represent the percent change (decimal) in residence time per standard deviation in observed forcing. The dominant forcing mechanism for each zone is bold.

cross-shore and alongshore momentum balances, (2) they do not require reducing the morphology of a complex coastal reef to a single representative cross-reef depth profile, and (3) the role of multiple forcing mechanisms (wave, wind, tide), including their often complex interactions, can be properly simulated. For this application we were fortunate to have very high-resolution LIDAR bathymetry data. Perhaps the greatest limitation to applying such models to other reef systems is the lack of comparable high-resolution bathymetry: an essential prerequisite for developing accurate 2D and 3D models.

5.3. Relative Importance of Physical Forcing and Its Spatial Variability

[36] Results from the particle tracking simulations revealed that residence times within Kaneohe Bay are extremely heterogeneous and influenced to varying degrees by wave, wind and tidal forcing (Figure 12 and Table 4). To investigate the relative importance of the various forcing mechanisms to the residence time T_{res} within each of the six zones defined within Kaneohe Bay (Figure 5), sensitivity parameters for each forcing were estimated by evaluating the percent change in residence time resulting from the standard deviation of historical forcing variability. Residence time sensitivities, were thus calculated as follows for tide (using runs P2−P3), wave (using P4−P5), and wind forcing (using P6−P7) respectively,

$$\frac{\sigma_a}{T_{res,0}}\frac{\partial T_{res}}{\partial a}, \frac{\sigma_{H_s}}{T_{res,0}}\frac{\partial T_{res}}{\partial H_s}, \frac{\sigma_{U_{wind}}}{T_{res,0}}\frac{\partial T_{res}}{\partial U_{wind}} \quad (4)$$

where a is the tidal range, H_s is the incident significant wave height, U_{wind} is the imposed wind speed, and the subscript "0" represents the value of a parameter under the default (average) forcing (i.e., from run P1; Table 4). The σs represent the standard deviation from ∼1 year of historical forcing data from *Lowe et al.* [2009]; that is, $\sigma_a = 0.21$ m for tidal range (because of spring-neap cycle variability), $\sigma_{H_s} = 0.54$ m for offshore significant wave height, and $\sigma_{U_{wind}} = 1.51$ m s^{-1} for wind speed. Hence, for example, to evaluate the particular sensitivity to wave forcing, the derivative in equation (4) was estimated as $\sim\Delta T_{res}/\Delta H_s$, on the basis of the difference in T_{res} computed between runs P4 and P5 and the difference in wave heights simulated (3 m).

[37] Table 5 reveals that the relative importance of the various forcing mechanisms varies markedly across the system, as expected. Although tidal forcing has only a minor influence on residence times throughout much of the system, tides play a dominant role in flushing the southern lagoon (i.e., zone 6) and influence the flushing of the channel region (zone 3) to some degree. In contrast, wave forcing is the dominant mechanism driving the circulation over most of the system (zones 1−2, 4−5). Residence times are generally much less influenced by wind forcing than wave forcing, however, a wind stress can contribute somewhat to the flushing of the northern lagoon and channel regions (zones 1 and 4) and also influences the residence time associated with the sluggish southern lagoon waters (zone 6).

6. Summary and Conclusions

[38] Wave transformations across the Kaneohe Bay reef-lagoon system modeled by SWAN using single-parameter values to describe bottom roughness and depth-limited wave breaking for the whole domain were in good agreement with observed wave heights. Wave forces produced by SWAN generated free surface changes that matched observations, albeit with less skill than the wave height predictions themselves. Nonetheless, Delft3D successfully predicted the magnitude and direction of currents using a spatially uniform hydraulic roughness length scale. Overall, the modeled changes in free-surface elevation show the importance of setup within the lagoon, which was a substantial fraction of the setup at the reef crest (∼50−70%). In conjunction with the relatively wide reef flat (∼1.5 km), this led to flows across the Kaneohe Bay reef flat that were weaker than wave-driven flows in excess of 50 cm s^{-1} that are typically observed on wave-exposed atolls and barrier reefs [*Gourlay and Colleter*, 2005]. The model did produce some small biases, including the overprediction of net currents in the channels as well as some underprediction of current variability on the reef flat. Nonetheless, the overall skill of the model in predicting currents was ∼0.65 for absolute speed and ∼0.92 based on the current variability alone.

[39] Residence times calculated by releasing passive particles under various forcing scenarios indicate that both the northwest region of the reef flat (zone 1) and the northwest section of the lagoon (zone 4) have residence times on the order of ∼1 day while the southeast extent of the reef flat (zone 3) has residence times of 2−5 days. The central part of the reef flat (zone 2) has residence times of ∼6 days, much longer than other sections of the reef flat. In this region a persistent onshore wave-driven flow is present, which transports a fraction of material across the reef that becomes entrained into the much more sluggish central lagoon waters. The central lagoon (zone 5) has longer residence times of ∼10 days due to its larger volume and physical separation from the coastal ocean; however, the

southern section of Kaneohe Bay (zone 6) has by far the longest residence times of 1–2 months. These extremely long residence times are due mainly to geographic isolation, its resistance to forcing by waves, and its connectivity with the rest of Kaneohe Bay being limited to just two narrow channels on either side of Coconut island. The southeast section of Kaneohe Bay should more appropriately be thought of as a secondary lagoon extending off of the primary lagoon (zones 4 and 5).

[40] As a final note, we believe that the use of 2D and 3D coupled wave-circulation numerical models such as Delft3D to studies of reef-lagoon systems offers numerous advantages over 1D models that have been much more frequently employed in studies of wave-driven reef circulation. This is particularly the case for systems such as Kaneohe Bay that are both morphologically complex also forced by multiple mechanisms (e.g., waves and tides), which results in a dynamic sea surface elevation that has inherent 2D structure (Figure 11). Although these coupled wave-circulation numerical models have primarily been tested on sandy beaches [e.g., *Lesser et al.*, 2004; *Newberger and Allen*, 2007; *Warner et al.*, 2008]], the fact that Delft3D performed well for Kaneohe Bay suggests that these models should perform equally well in simulations of wave transformation and circulation in other similar coastal reef-lagoon systems or rocky shorelines. We caution that the Kaneohe forereef slope (~1:60), as well as the forereef slope of many coastal fringing reefs, is very similar to many beaches and notably much milder than the nearly vertical faces encountered on many Indo-Pacific atolls and barrier reefs [*Gourlay and Colleter*, 2005]. For these very steep reefs, the mild slope assumptions used to parameterize wave transformation and setup within existing numerical models will likely breakdown; thus, further work is ultimately required to develop appropriate numerical tools to properly simulate wave-driven flows over this particular class of steep reefs.

[41] **Acknowledgments.** We are especially grateful to Ap Van Dongeren and Dano Roelvink for the many helpful discussions while the model was developed. This work was supported by the National Science Foundation through grants OCE-0452800, OCE-0453117, and OISE-0601787. RJL acknowledges support from an Australian Research Council Discovery Project grant DP0770094. Use of the model is gratefully acknowledged as part of the Delft3D Community Model Development Project sponsored by WL|Delft Hydraulics and the U.S. Office of Naval Research.

References

Alford, M. H., M. C. Gregg, and M. A. Merrifield (2006), Structure, propagation, and mixing of energetic baroclinic tides in Mamala Bay, Oahu, Hawaii, *J. Phys. Oceanogr.*, *36*, 997–1018, doi:10.1175/JPO2877.1.

Andrews, J. C., and G. L. Pickard (1990), The physical oceanography of coral reef systems, in *Coral Reefs*, edited by Z. Dubinsky, chap. 2, pp. 11–48, Elsevier, Amsterdam.

Angwenyi, C. M., and L. Rydberg (2005), Wave-driven circulation across the coral reef at Bamburi Lagoon, Kenya, *Estuarine Coastal Shelf Sci.*, *63*, 447–454, doi:10.1016/j.ecss.2004.12.008.

Atkinson, M. J., and R. W. Bilger (1992), Effects of water velocity on phosphate uptake in coral reef-flat communities, *Limnol. Oceanogr.*, *37*, 273–279.

Battjes, J. A., and J. P. F. M. Janssen (1978), Energy loss and set-up due to breaking of random waves, in *Coastal Engineering (1978 Germany)*, pp. 569–587, Am. Soc. of Civ. Eng., New York.

Battjes, J. A., and M. J. F. Stive (1985), Calibration and verification of a dissipation model for random breaking waves, *J. Geophys. Res.*, *90*, 9159–9167, doi:10.1029/JC090iC05p09159.

Beardsley, R. C., R. Limeburner, and L. K. Rosenfeld (1985), Introduction to the CODE-2 moored array and large-scale data report, in *CODE-2: Moored Array and Large-Scale Data Report*, edited by R. Limeburner, *CODE Tech. Rep. 38, WHOI Tech. Rep. 85-35*, 234 pp., Woods Hole Oceanogr. Inst., Woods Hole, Mass.

Booij, N., R. C. Ris, and L. H. Holthuijsen (1999), A third-generation wave model for coastal regions: 1. Model description and validation, *J. Geophys. Res.*, *104*, 7649–7666, doi:10.1029/98JC02622.

Deigaard, R., et al. (1986), Suspended sediment in the surf zone, *J. Waterw. Port Coastal Ocean Eng.*, *112*, 115–128.

Dingemans, M. W., A. C. Radder, and H. J. DeVriend (1987), Computation of the driving forces of wave-induced currents, *Coastal Eng.*, *11*, 539–563, doi:10.1016/0378-3839(87)90026-3.

Douillet, P., et al. (2001), A numerical model for fine suspended sediment transport in the southwest lagoon of New Caledonia, *Coral Reefs*, *20*, 361–372, doi:10.1007/s00338-001-0193-6.

Falter, J. L., R. J. Lowe, M. J. Atkinson, S. G. Monismith, and D. W. Schar (2008), Continuous measurements of net production over a shallow reef community using a modified Eulerian approach, *J. Geophys. Res.*, *113*, C07035, doi:10.1029/2007JC004663.

Fredsoe, J. (1984), Turbulent boundary-layer in wave-current motion, *J. Hydraul. Eng.*, *110*, 1103–1120, doi:10.1061/(ASCE)0733-9429(1984)110:8(1103).

Gourlay, M. R., and G. Colleter (2005), Wave-generated flow on coral reefs: An analysis for two dimensional horizontal reef-tops with steep faces, *Coastal Eng.*, *52*, 353–387, doi:10.1016/j.coastaleng.2004.11.007.

Hearn, C. J. (1996), Application of the model SPECIES to Kaneohe Bay, Oahu, Hawaii, in *Estuarine and Coastal Modeling 1995*, pp. 355–366, Am. Soc. of Civ. Eng., New York.

Hearn, C. J. (1999), Wave-breaking hydrodynamics within coral reef systems and the effect of changing relative sea level, *J. Geophys. Res.*, *104*, 30,007–30,019, doi:10.1029/1999JC900262.

Hench, J. L., J. L. Leichter, and S. G. Monismith (2008), Episodic circulation and exchange in a wave driven coral reef and lagoon system, *Limnol. Oceanogr.*, *53*, 2681–2694.

Jokiel, P. (2008), Biological and ecological functioning of coral reefs in the main Hawaiian Islands, in *Coral Reefs of the USA*, edited by B. Reigl and R. Dodge, pp. 489–518, Springer, Dordrecht, Germany.

Jones, N. J., R. J. Lowe, D. A. Fong, G. Pawlak, and S. G. Monismith (2008), Plume dispersion on a fringing coral reef system, *Limnol. Oceanogr.*, *53*, 2273–2286.

Jonsson, I. G. (1966), Wave boundary layers and friction factors1966, *Coastal Engineering (1966)*, pp. 127–148, Am. Soc. of Civ. Eng., New York.

Jouon, A., et al. (2006), Calculations of hydrodynamic time parameters in a semi-opened coastal zone using a 3D hydrodynamic model, *Cont. Shelf Res.*, *26*, 1395–1415, doi:10.1016/j.csr.2005.11.014.

Kench, P. S., and R. W. Brander (2006), Wave processes on coral reef flats: Implications for reef geomorphology using Australian case studies, *J. Coastal Res.*, *22*, 209–223, doi:10.2112/05A-0016.1.

Kitheka, J. U. (1997), Coastal tidally driven circulation and the role of water exchange in the linkage between tropical coastal ecosystems, *Estuarine Coastal Shelf Sci.*, *45*, 177–187, doi:10.1006/ecss.1996.0189.

Kraines, S. B., et al. (1998), Wind-wave driven circulation on the coral reef at Bora Bay, Miyako Island, *Coral Reefs*, *17*, 133–143, doi:10.1007/s003380050107.

Kraines, S. B., A. Suzuki, T. Yanagi, M. Isobe, X. Guo, and H. Komiyama (1999), Rapid water exchange between the lagoon and the open ocean at Majuro Atoll due to wind, waves, and tide, *J. Geophys. Res.*, *104*, 15,635–15,653, doi:10.1029/1999JC900065.

Kraines, S. B., et al. (2001), Seasonal variations in the exchange of water and water-borne particles at Majuro Atoll, the Republic of the Marshall Islands, *Coral Reefs*, *20*, 330–340, doi:10.1007/s00338-001-0191-8.

Lesser, G. R., et al. (2004), Development and validation of a three-dimensional morphological model, *Coastal Eng.*, *51*, 883–915, doi:10.1016/j.coastaleng.2004.07.014.

Lowe, R. J., J. L. Falter, M. D. Bandet, G. Pawlak, M. J. Atkinson, S. G. Monismith, and J. R. Koseff (2005), Spectral wave dissipation over a barrier reef, *J. Geophys. Res.*, *110*, C04001, doi:10.1029/2004JC002711.

Lowe, R. J., et al. (2008), Modeling flow in coral communities with and without waves: A synthesis of porous media and canopy flow approaches, *Limnol. Oceanogr.*, *53*, 2668–2680.

Lowe, R. J., et al. (2009), Wave-driven circulation of a coastal reef-lagoon system, *J. Phys. Oceanogr.*, *39*, 873–893, doi:10.1175/2008JPO3958.1.

Lugo-Fernandez, A., H. H. Roberts, W. J. Wiseman, and B. L. Carter (1998), Water level and currents of tidal and infragravity periods at Tague Reef, St. Croix (USVI), *Coral Reefs*, *17*, 343–349, doi:10.1007/s003380050137.

Lugo-Fernandez, A., et al. (2001), Inferring probable dispersal of Flower Garden Banks Coral Larvae (Gulf of Mexico) using observed and simu-

lated drifter trajectories, *Cont. Shelf Res.*, *21*, 47–67, doi:10.1016/S0278-4343(00)00072-8.

Lugo-Fernandez, A., et al. (2004), Currents, water levels, and mass transport over a modern Caribbean coral reef: Tague Reef, St Croix, USVI, *Cont. Shelf Res.*, *24*, 1989–2009, doi:10.1016/j.csr.2004.07.004.

Luick, J. L., et al. (2007), Circulation in the Great Barrier Reef Lagoon using numerical tracers and in situ data, *Cont. Shelf Res.*, *27*, 757–778, doi:10.1016/j.csr.2006.11.020.

MacMahan, J. H., et al. (2006), Rip current review, *Coastal Eng.*, *53*, 191–208, doi:10.1016/j.coastaleng.2005.10.009.

Madsen, O. S., et al. (1988), Spectral wave attenuation by bottom friction: Theory, in *Coastal Engineering 1988*, pp. 492–504, Am. Soc. of Civ. Eng., New York.

Mellor, G. (2003), The three-dimensional current and surface wave equations, *J. Phys. Oceanogr.*, *33*, 1978–1989, doi:10.1175/1520-0485(2003)033<1978:TTCASW>2.0.CO;2.

Monismith, S. G. (2007), Hydrodynamics of Coral Reefs, *Annu. Rev. Fluid Mech.*, *39*, 37–55, doi:10.1146/annurev.fluid.38.050304.092125.

Monismith, S. G., A. Genin, M. A. Reidenbach, G. Yahel, and J. R. Koseff (2006), Thermally driven exchanges between a coral reef and the adjoining ocean, *J. Phys. Oceanogr.*, *36*, 1332–1347, doi:10.1175/JPO2916.1.

Monsen, N. E., et al. (2002), A comment on the use of flushing time, residence time, and age as transport time scales, *Limnol. Oceanogr.*, *47*, 1545–1553.

Newberger, P. A., and J. S. Allen (2007), Forcing a three-dimensional, hydrostatic, primitive-equation model for application in the surf zone: 1. Formulation, *J. Geophys. Res.*, *112*, C08018, doi:10.1029/2006JC003472.

Nielsen, P. (1992), *Coastal Bottom Boundary Layers and Sediment Transport*, 324 pp., World Sci., River Edge, N. J.

Pawlowicz, R., B. Beardsley, and S. Lentz (2002), Classical tidal harmonic analysis including error estimates in MATLAB using T_TIDE, *Comput. Geosci.*, *28*, 929–937, doi:10.1016/S0098-3004(02)00013-4.

Pinazo, C., et al. (2004), Impact of wind and freshwater inputs on phytoplankton biomass in the coral reef lagoon of New Caledonia during the summer cyclonic period: A coupled three-dimensional biogeochemical modeling approach, *Coral Reefs*, *23*, 281–296, doi:10.1007/s00338-004-0378-x.

Prager, E. J. (1991), Numerical simulation of circulation in a Carribean-type backreef lagoon, *Coral Reefs*, *10*, 177–182, doi:10.1007/BF00336771.

Reidenbach, M. A., S. G. Monismith, J. R. Koseff, G. Yahel, and A. Genin (2006), Boundary layer turbulence and flow structure over a fringing coral reef, *Limnol. Oceanogr.*, *51*, 1956–1968.

Roelvink, J. A., and D. J. R. Walstra (2004), Keeping it simple by using complex models, in *Advances in Hydro-Science and Engineering*, vol. VI, edited by M. S. Altinakar et al., pp. 1–11, Univ. of Miss, University.

Smith, S. D., and E. G. Banke (1975), Variation of the sea surface drag coefficient with wind speed, *Q. J. R. Meteorol. Soc.*, *101*, 665–673, doi:10.1002/qj.49710142920.

Spagnol, S., et al. (2002), An error frequently made in the evaluation of advective transport in two-dimensional Lagrangian models of advection-diffusion in coral reef waters, *Mar. Ecol. Prog. Ser.*, *235*, 299–302, doi:10.3354/meps235299.

Storlazzi, C. D., et al. (2004), Wave- and tidally driven flow and sediment flux across a fringing coral reef: Southern Molokai, Hawaii, *Cont. Shelf Res.*, *24*, 1397–1419, doi:10.1016/j.csr.2004.02.010.

Symonds, G., K. P. Black, and I. R. Young (1995), Wave-driven flow over shallow reefs, *J. Geophys. Res.*, *100*, 2639–2648.

Tartinville, B., et al. (1997), The water residence time in the Mururoa atoll lagoon: Sensitivity analysis of a three-dimensional model, *Coral Reefs*, *16*, 193–203, doi:10.1007/s003380050074.

van den Boogaard, H. F. P., M. J. J. Hoogkamer, and A. W. Heemink (1993), Parameter identification in particle models, *Stochastic Hydrol. Hydraul.*, *7*, 109–130, doi:10.1007/BF01581420.

Walstra, D. J. R., J. A. Roelvink, and J. Groeneweg (2000), Calculation of wave-driven currents in a 3D mean flow model, in *Coastal Engineering (2000)*, edited by B. L. Edge, pp. 1050–1063, doi:10.1061/40549(276)81.

Warner, J. C., W. R. Geyer, and J. A. Lerczak (2005), Numerical modeling of an estuary: A comprehensive skill assessment, *J. Geophys. Res.*, *110*, C05001, doi:10.1029/2004JC002691.

Warner, J. C., et al. (2008), Development of a three-dimensional, regional, coupled wave, current, and sediment transport model, *Comput. Geosci.*, *34*, 1284–1306, doi:10.1016/j.cageo.2008.02.012.

Willmott, C. J., et al. (1982), Some comments on the evaluation of model performance, *Bull. Am. Meteorol. Soc.*, *63*, 1309–1313, doi:10.1175/1520-0477(1982)063<1309:SCOTEO>2.0.CO;2.

Yahel, G., et al. (1998), Phytoplankton distribution and grazing near coral reefs, *Limnol. Oceanogr.*, *43*, 551–563.

Yamano, H., et al. (1998), Water circulation in a fringing reef located in a monsoon area: Kabira Reef, Ishigaki Island, southwest Japan, *Coral Reefs*, *17*, 89–99, doi:10.1007/s003380050101.

M. J. Atkinson and J. L. Falter, Hawai'i Institute of Marine Biology, University of Hawai'i, Kaneohe, HI 96744, USA.

R. J. Lowe, School of Earth and Environment, University of Western Australia, Crawley, WA 6009, Australia. (ryan.lowe@uwa.edu.au)

S. G. Monismith, Environmental Fluid Mechanics Laboratory, Stanford University, Stanford, CA 94305–4020, USA.